






Lunar Occultations with Aqueye+ and Iqueye

Luca Zampieri¹ , Andrea Richichi² , Giampiero Naletto^{1,3}, Cesare Barbieri^{1,3}, Aleksandr Burtovoi^{1,4}, Michele Fiori^{1,3}, Andreas Glindemann⁵, Gabriele Umbriaco³, Paolo Ochner^{1,3}, Vladimir V. Dyachenko⁶, and Mauro Barbieri⁷ 

¹INAF—Astronomical Observatory of Padova Vicolo dell’Osservatorio 5, I-35122 Padova, Italy; luca.zampieri@oapd.inaf.it

²INAF—Astronomical Observatory of Arcetri Largo E. Fermi 5, I-50125 Firenze, Italy

³Department of Physics and Astronomy, University of Padova Via F. Marzolo 8, I-35131 Padova, Italy

⁴Center of Studies and Activities for Space (CISAS) “G. Colombo,” University of Padova Via Venezia 15, I-35131 Padova, Italy

⁵European Southern Observatory Karl-Schwarzschild-StraÙe 2, D-85748 Garching bei München, Germany

⁶Special Astrophysical Observatory Nizhniy Arkhyz, 369167 Karachai-Cherkessian Republic, Russia

⁷Instituto de Astronomía y Ciencias Planetarias (INCT), University of Atacama, Avenida Copayapu 485, 1531772 Copiapó, Atacama, Chile

Received 2018 October 15; revised 2019 August 6; accepted 2019 August 6; published 2019 October 10

Abstract

We report the first-time use of the Aqueye+ and Iqueye instruments to record lunar occultation events. High time resolution recordings in different filters have been acquired for several occultations taken from 2016 January through 2018 January with Aqueye+ at the Copernicus telescope and Iqueye at the Galileo telescope in Asiago, Italy. Light curves with different time bins were calculated in post-processing and analyzed using a least-square model-dependent method. A total of nine occultation light curves were recorded, including one star for which we could measure for the first time the size of the chromosphere (μ Psc) and one binary star for which discrepant previous determinations existed in the literature (SAO 92922). A disappearance of Alf Tau shows an angular diameter in good agreement with literature values. The other stars were found to be unresolved, at the milliarcsecond level. We discuss the unique properties of Aqueye+ and Iqueye for these kind of observations, namely the simultaneous measurement in up to four different filters thanks to pupil splitting, and the unprecedented time resolution well exceeding the microsecond level. This latter makes Aqueye+ and Iqueye suitable to observe not just occultations by the Moon, but also much faster events such as, e.g., occultations by artificial screens in low orbits. We provide an outlook of future possible observations in this context.

Key words: binaries: general – occultations – stars: fundamental parameters – techniques: high angular resolution

1. Introduction

Lunar occultations (LO) have played a major role in high angular resolution astronomy in the past several decades, thanks to the ability to use the quantitative details of the diffraction pattern generated at the Moon’s limb to retrieve information on the occulted source on the milliarcsecond (mas) level. The technique has been very successful in spite of several important limitations, e.g., that LO are fixed time events, that the sources cannot be chosen at will, and that only 1D information can be retrieved (unless simultaneous measurements taken at different sites are available). A compilation of LO results, including pioneering works such as those of Africano et al. (1978), Ridgway et al. (1982), and Schmidtke et al. (1986), can be found in the update of the Catalog of High Angular Resolution Measurements (CHARM2; Richichi et al. 2005). In the last few years, LO have been exploited at an increasing number of observatories, both in the near-IR and in the visual thanks to the ability to reach the required millisecond time resolutions on standard astronomical detectors read-out in subarray modes (see Richichi et al. 2014, 2016, 2017a, and references therein). The relatively simple required instrumentation and data analysis and, in some cases, the possibility to recover complex brightness profiles, make the LO technique still competitive, e.g., in comparison with long-baseline or speckle interferometry. More recently, occultation events from the Saturnian ring plane recorded with the *Cassini* spacecraft were used to perform novel observations in the near-IR (Stewart et al. 2013, 2015, 2016). Another very interesting extension of the occultation technique has been recently reported by Benbow et al. (2019). They used the 12 m

VERITAS telescopes and an occulting asteroid rather than the Moon to measure stellar diameters with an impressive resolution of ≤ 0.1 mas.

In this context, we report on the first LO observations by Aqueye+ and Iqueye, two similar instruments primarily designed for very high time resolution astrophysics and quantum astronomy (Barbieri et al. 2009; Naletto et al. 2009, 2013; Verroi et al. 2013; Zampieri et al. 2015, 2016). Aqueye+ and Iqueye couple the ultra-high time resolution of single-photon avalanche photodiode (SPAD) detectors with a split-pupil optical concept and an extremely accurate timing system. The arrival time of each individual photon is determined with < 500 ps absolute time accuracy with respect to UTC. We have observed a total of nine LO events, leading to the measurement of one resolved angular diameter and one small separation binary source, as well as to the confirmation of Alf Tau’s angular size. This initial sample has allowed us to establish the performance of these instruments on the Asiago telescopes for LO observations, and to plan for future use considering also that Iqueye is designed to be easily mounted at other telescopes. We also discuss the benefits granted by the pupil-plane splitting design of A/Iqueye, which enables recording light curves in up to four independent filters, and by the possible simultaneous use at two different Asiago telescopes. A/Iqueye allow for time resolutions as fast as a fraction of a nanosecond, arguably the fastest available at present in astronomical instrumentation, being originally designed for performing experiments in the field of quantum astronomy, including stellar intensity interferometry (Zampieri et al. 2016). While this is not needed for standard occultations by the Moon, where light curve sampling at the millisecond

Table 1
List of Observed Events

Date	Time (UT)	Config.	Source	V (mag)	Sp	Filter1	Filter2	S/N	Notes
2016 Jan 16	18:57	A-1.8m	μ Psc	4.8	K4III	H_{α}	4xnil	25.6	Diam
2016 Jan 17	18:38	A-1.8m	SAO 92922	7.1	K0	H_{α}	4xnil	4.5	Bin
2016 Dec 6	18:59	I-1.2m	SAO 146200	8.9	M1III	R	4xnil	5.5	UR
2016 Dec 6	19:33	I-1.2m	SAO 146213	9.5	G5V	R	4xnil	1.8	UR
2016 Dec 7	18:47	I-1.2m	SAO 146724	7.0	K4/5III	R	3xnil, 610	21.8	UR
2016 Dec 7	20:14	I-1.2m	SAO 146747	8.0	K0III	R	2xnil, 546, 610	6.7	UR
2016 Dec 7	20:24	I-1.2m	SAO 146750	9.5	K5	R	2xnil, 546, 610	3.4	UR
2017 Dec 31	01:37	I-1.2m	α Tau	0.9	K5+III	H_{α}	4xnil	23.2	Diam
2018 Jan 25	17:55	I-1.2m	IRC+10035	5.9	K6	I	4xnil	16.7	UR

level is sufficient, we discuss the exciting prospect of recording occultations by other types of screens.

In Section 2 we present the observations and we briefly summarize the data analysis, based on well-established previous work. In Sections 3 and 4 we show our results and discuss the specific advantages of Aqueye+ and Iqueye for this type of observation, as well as their potential for non-LOs such as from artificial screens. Finally, in Section 5 we give some concluding remarks.

2. Observations and Data Analysis

All observations reported here were recorded with Iqueye installed at the 1.22 m Galileo telescope located on the grounds of the Asiago Observatory in northern Italy, or with Aqueye+ on the 1.82 m Copernico telescope located about 4 km away at Cima Ekar. Iqueye is fed through an optical fiber mounted on a dedicated opto-mechanical interface (Iqueye Fiber Interface, IFI) attached to the Nasmyth focus of the 1.22 m Galileo telescope (Zampieri et al. 2016).

The journal of the observations is provided in Table 1. All events were disappearances on the dark limb of the Moon. The first few columns list the date, time, instrument and telescope combination, source designation, magnitude, and spectrum. These latter were compiled from the *Simbad* database (Wenger et al. 2000).

As discussed in Section 4, A/Iqueye has a characteristic optical design that splits the beam into four channels, each sensed by a dedicated SPAD. A filter wheel is placed on the entrance beam, and thus common to all channels, while additional filters are available on each channel. In the main wheel we inserted either a nonstandard R filter with a FWHM ≈ 150 nm, or an I filter with FWHM ≈ 100 nm, or a H_{α} filter with FWHM ≈ 3 nm. These FWHM already include the SPAD response. On the secondary wheels we selected the open position or additional independent filters. These settings are denoted by Filter1 and Filter2 in Table 1, where we used nil when no filter was inserted. The 546 and 610 are the central wavelengths in nanometers of the secondary filters, both with 10 nm FWHM. So in the case of SAO 146724, e.g., three channels were recorded in a R filter, and one in a $R+610$ nm filter. However, these narrow filters are outside or just at the beginning of the R filter passband. They were inserted only to be used with other concurrent observations. For our specific case, they gave a nonsignificant signal and were not considered in the data analysis.

The A/Iqueye data are in the form of a stream of photon counts, each with their time tag at the sub-nanosecond accuracy level. For the present purpose, all channels have been rebinned

to 2.5 ms, and only those with non-zero signal (see above) have been averaged to obtain a single light curve. The last two columns of the table denote the signal-to-noise ratio (S/N) of the best model fit to the data, and whether the source was found to be resolved, binary, or unresolved.

The light curves obtained in this way were trimmed to a few seconds around the event, and then analyzed using a least-square model-dependent (LSM) method, the details of which are given in Richichi et al. (1992). This approach uses a uniform disk (UD) model of the stellar disk with its angular diameter as a free parameter. Convergence in χ^2 is based on a noise model built from data before and after the occultation, with parameters such as read-out noise, detector gain, and level of scintillation (see Richichi 1989). Scintillation can be interpolated to some extent by Legendre polynomials. This LSM method is also used in the case of binary stars, with projected separations and individual fluxes as additional free parameters. In addition, we also used the so-called CAL method (Richichi 1989) to derive model-independent brightness profiles. This method applies an iterative deconvolution to retrieve the most likely solution to the profile, and is particularly useful to detect small separation binaries.

3. Results

3.1. μ Psc

The light curve for the LO of this K3–K4 giant (HR 434, IRC+10017) is shown in Figure 1. Our data are best fitted with a UD model of 3.14 ± 0.05 mas diameter (radius $34.2 \pm 1.2 R_{\odot}$ using the *Gaia* parallax of 9.85 ± 0.32 mas; *Gaia* Collaboration et al. 2018). The light curve in Figure 1 is obtained summing together the photons from all channels. A consistent result (within the errors) is found analyzing the light curves from the four channels individually, and then averaging the measurements (see Section 4).

Beavers et al. (1982) had also resolved this star by LO simultaneously in blue and red filters. Although the two measurements had rather different values, their average was 3.3 ± 1.0 mas, loosely consistent with expectations and with our determination too. Indirect estimates using the infrared flux method provide however smaller values, ranging between 2.58 and 2.77 mas with errors at the 1%–3% level (Bell & Gustafsson 1989; Blackwell et al. 1990; Cohen et al. 1999). These are reported for a limb-darkened (LD) diameter, rather than a UD diameter. However, for the effective temperature, surface gravity, and metallicity of μ Psc (K3–K4 giant; McWilliam 1990), the expected LD/UD correction at our LO data wavelength is of an order of 1.2% (Davis et al. 2000), and therefore negligible against other uncertainties in our specific

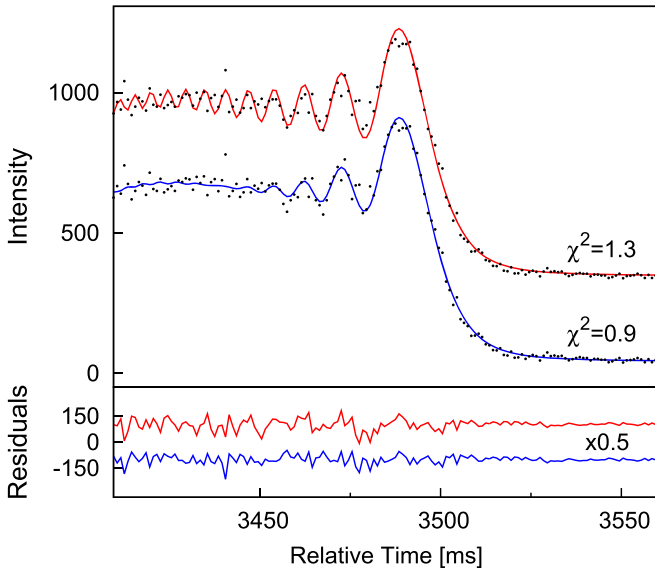


Figure 1. Top panel: light curve (dots) for μ Psc, repeated twice with an arbitrary offset. The upper solid line is a fit with a point-like source, the lower solid line is the best fit with a UD model. The best fitting value of the diameter is 3.14 ± 0.05 mas. The reduced χ^2 values for the two cases are also shown. The improvement of the fit is highly significant ($\Delta \chi^2 > 30$ for one additional degree of freedom). Bottom panel: the residuals for the two fits, offset by arbitrary amounts and rescaled for clarity.

case. Our angular diameter determination thus appears to be about 15% larger than expected, with a 5σ significance.

To explain such a significant difference we note that the two methods have sampled different optical depths of the star. Namely, the infrared flux method provides an estimate in the continuum and thus of the photospheric disk, while our LO measurement returns the stellar diameter in H_α . According to Mauas et al. (2006) and Vieytes et al. (2011), in K giants the core of the H_α line is formed at heights ranging from 20%–30% to 100% above the photosphere. To check the possibility that we detected the chromosphere of the star, we acquired a medium resolution spectrum of μ Psc with the Boller & Chivens (B&C) spectrograph at the Galileo telescope in Asiago in late 2017. This was significantly later than the LO event, but no significant variability is known for this star. The spectrum shows a strong absorption H_α line with a FWHM of ≈ 0.2 nm, or 15 times narrower than our filter bandwidth. The difference between the line width and the filter bandpass implies that our LO measurement is probably underestimating the actual chromospheric diameter, being largely contaminated by the photospheric emission. This is consistent with our finding that the chromospheric diameter is only about 15% larger than the photospheric disk, to be compared with a value potentially as high as 100%, as already stated. To provide more insight into this intriguing measurement, further modeling including higher spectral resolution and atmospheric simulations would be desirable.

3.2. SAO 92922

This star (HD 14866, HIP 11194) was first reported as a possible LO double by Edwards et al. (1980). However, a subsequent LO event along a very similar position angle did not find duplicity (Schmidtke & Africano 1984). Following that, a number of measurements by speckle interferometry resulted in a few detections of the binary component

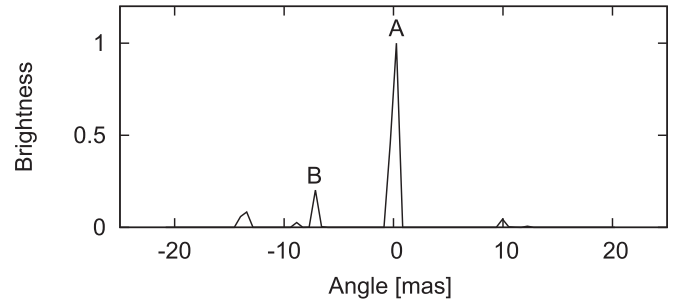


Figure 2. Brightness profile of SAO 92922 derived from our LO light curve using the method described in the text. Two peaks are clearly detected (A and B), indicating the existence of two components.

(Mason 1996; Mason et al. 2001), but also yielded several nondetections as well. The authors justified this with the presumably high magnitude difference.

Richichi et al. (2017b) succeeded in resolving the binary by LO. Just a few weeks later we observed the event reported in this paper. As for μ Psc, the light curve was derived summing together the photons from all channels. A consistent result (within the errors) is found analyzing the light curves from the four channels individually, and then averaging the measurements (see Section 4). The light curve was analyzed using the CAL method mentioned in Section 2, and the result is shown in Figure 2. The detection of a second component in the brightness profile (B component) is statistically significant, when compared against the noise baseline level (a few percent), as seen in Figure 2. The light curve was thus fitted using the LSM method, and a two-component model.

Given that our measurement and that of Richichi et al. (2017b) were relatively close in time, we could neglect orbital motion and combine the two projections to yield an on-sky separation of 13.7 ± 1.0 mas and position angle of 71.3 ± 2.8 . The error on this latter quantity was computed assuming an error of 5° on the position angle of each occultation event, since the S/N was not sufficient to determine the local limb slope for either one. More specifically, the values and errors of the separation and position angle are obtained using a program which finds the solution from numerical steps in each parameter and propagates the errors. In general, this needs some input values and their errors. Since in this case a fit-derived error on the position angles of the measurements was not available, we adopted 5° as an acceptable guess for the projected individual errors.

We followed up this system with extensive speckle observations from the Russian 6 m telescope on 2017 December 16 (for a description of the EMCCD-based speckle interferometer of the BTA 6 m telescope, see Maksimov et al. 2009). Several filters were used, that are listed below with their central wavelength and FWHM in nanometers. The observations were repeated up to 6 hr apart, allowing for significant changes in parallactic angle and thus in possible instrumental signatures. The system was found to be unresolved. The following upper limits on the separation refer to a companion with 0 and 3 mag brightness difference. Filter 450/25: 50–60 mas; 550/20: 20–35 mas; 700/50: 25–40 mas; 800/100: 30–50 mas. These values are larger than, and thus not inconsistent with, the ≈ 14 mas true separation found from our combined LO observations less than one year earlier. We note that these results depend not only on the wavelength (which indeed determines the diffraction limit) and bandpass,

Table 2
List of Measurements of the Binary SAO 92922

Ref.	Date	ΔT (yr)	Method	Detect	Sep (mas)	PA	Filter	Δm	Notes
Edwards et al. (1980)	07-01-79	0.000	LO	Y?	31 ^P	229°9	Red	2.8	(1)
Schmidtke & Africano (1984)	25-09-83	4.715	LO	N		235°5	V		
Mason (1996)	08-11-85	6.838	SI	N			549/22		
Mason (1996)	14-09-94	15.687	SI	Y	131	184°1	549/22	N/A	
Mason (1996)	14-09-94	15.687	SI	N			700/40		
Mason (1996)	08-10-95	16.752	SI	Y	98	165°2	549/22	N/A	
Mason (1996)	08-10-95	16.752	SI	N			538/76		
Mason et al. (2001)	09-09-98	19.674	SI	Y	233	155°8	N/A	N/A	
Richichi et al. (2017b)	21-12-15	36.953	LO	Y	8.3 ± 0.2^P	304°	z'	1.41	(2)
This work	17-01-16	37.027	LO	Y	7.0 ± 0.8^P	192°	H_α	1.59	(2)
Previous two	03-01-16	36.990	LO	Comb	13.7 ± 1.0	251°3			(3)
This work	16-12-17	38.940	SI	N	<25–60		various	0–3	(4)

Note. Sep values followed by ^P are projected separations along the position angle. (1) No slope determination; not detected in blue channel. (2) No slope determination. (3) Geometrical combination, neglecting orbital motion and assuming a 5° error on the position angle. (4) See the text for details of filters and individual upper limits.

but also on the S/N, which in turn, depends on the system response including the detector. In this respect, the most stringent limit is set by the 550/20 observations where the telescope and CCD have peak response, rather than by the 450/25 observations which have a better diffraction limit but worse atmospheric speckle response and CCD quantum efficiency.

Table 2 reports the details of the measurements covering all observations back to those of Edwards et al. (1980), spanning an interval of almost 39 yr. It can be noted that the true separations appear to span a wide range. Although the 1995 and 1998 speckle interferometry (SI) measurements should be considered uncertain (B. Mason, private communication), we attempted to determine if any combination of the available detections is consistent with a plausible orbit. We then performed fits of all the measurements with binary orbits projected on the sky. We used the *Gaia* provided distance of $\simeq 120$ pc (Gaia Collaboration et al. 2018) and assumed a mass of $\sim 0.6 M_\odot$ for the primary and of $\sim 0.4 M_\odot$ for the secondary. The total mass of the binary is then $\sim 1 M_\odot$. No plausible orbit is in agreement with all measurements. Neglecting the widest measured separation (Mason et al. 2001), we found that orbits with inclination $\gtrsim 45^\circ$ – 60° and/or eccentricity $\gtrsim 0.1$ – 0.3 can reproduce the other three measurements for orbital periods in the interval of ~ 25 – 120 yr. However, the epoch of the two 1996 measurements (Mason 1996) are much more closely spaced (~ 1 yr) than predicted (~ 7 – 90 yr). In the same assumptions, orbits with any inclination and contained eccentricity (< 0.3) are in agreement within the errors with our measurement alone for orbital periods between ~ 2 and ~ 45 yr.

3.3. α Tau

Thanks to its proximity, brightness, and large angular size, this K5 giant has been extensively measured with several techniques. Based on near-IR measurements by occultations and interferometry, Richichi & Roccatagliata (2005) reported a limb-darkened diameter of 20.58 ± 0.03 mas. Accurate measurements remain however of high interest, because there are indications that the photosphere may not be completely symmetric (Richichi et al. 2017a).

We could record an event for α Tau in 2017 December, among the last ones of the series which just concluded in early

2018, in spite of the rather low elevation, high lunar phase, and high contact angle. The observation was carried out in H_α with the aim of searching for deviations from the photospheric angular diameter. Unfortunately, our data are limited in S/N due also to the reasons outlined in Section 3.4, and do not lend themselves to a detailed investigation of possible departures from a symmetric disk model. We can only conclude that a 20.6 mas symmetric model is in excellent agreement with the data, if one allows for a -5.8% deviation in limb speed from the predicted value. This is shown in Figure 3, where the fit additionally included also a scintillation correction using a 5th degree Legendre polynomial (Richichi et al. 1992). Adopting this limb speed would in turn lead to a -1.6 local limb slope, perfectly within the norm. Conversely, fixing the limb speed to the predicted value would result in an angular diameter of 21.7 ± 0.1 mas with similar fit quality (the standard deviation from the best fitting model is comparable in the two cases). This value would be significantly ($\sim 5\%$) larger than the limb-darkened diameter. Indeed, α Tau, at μ Psc, is a K giant and, similarly, the core of the H_α line forms well above the photosphere. We would have then detected the chromosphere of the star, although our inability to constrain the limb speed from the fit prevents us from reaching a definite conclusion.

3.4. Other Stars

The remaining stars in Table 1 were found to be single and unresolved, in accordance with previous angular diameter estimations which were in almost all cases < 1 mas. Only for IRC+10035 was the previous estimate significantly larger, namely 2.3 mas. Our data led to an upper limit of 2.1 ± 0.4 mas, limited by the S/N. Among these unresolved stars, the brightest is SAO 146724, which was recorded with an S/N similar to that of μ Psc. Indeed, the brightness difference of ≈ 2 mag between these two stars is roughly consistent with the FWHM difference between the filters (a factor of ~ 30) multiplied by the ratio of the telescope areas used in the two cases (a factor of ~ 0.4). However, we note that the scintillation level was more than 3% in the case of μ Psc. Our data show that $S/N \approx 30$ could be an ultimate limit for our setup.

As for sensitivity, the result achieved on SAO 146213 indicates that at 2.5 ms in a broadband filter the limiting magnitude should be between 9 and 10, depending on which of

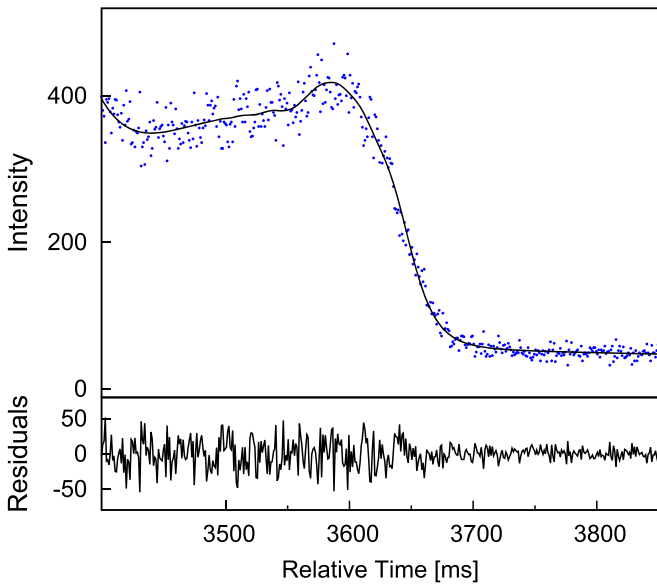


Figure 3. Top panel shows the light curve for α Tau, and the best fit using an ad hoc limb rate and a correction for scintillation as explained in the text. The fit residuals are shown in the bottom panel. The noise is greater before the star disappearance because of scintillation (after disappearance only diffuse emission is present).

the two Asiago telescopes is used. The LO event for this star was recorded with a moderate lunar phase but at a rather high airmass.

4. Specific Advantages of A/Iqueye for Occultations

A/Iqueye were developed mostly for different purposes than LO. We essentially used what was available and applied it to LO, without changing the instrument setup. This fact leads to interesting advantages, but also to some issues that we needed to test. The possibility to bin the data over a wide, user-selected range of sampling rates according to the brightness of the source and the intended science goal is clearly an advantage of A/Iqueye over most other instruments used for LO work. An additional feature, as already discussed, is pupil splitting, the merits of which for our original scientific drivers is described in previous work (Barbieri et al. 2009; Naletto et al. 2009, 2013; Zampieri et al. 2015). The beam is split by means of a pyramid mirror into four channels, each sensed by a dedicated SPAD. In principle, this setup allows us to perform simultaneous LO measurements with up to four independent filters. These types of measurements were already done in the past using a gray beam splitter or dichroic beam splitters, but at present A/Iqueye are the only instrumentation implementing this important observing mode of operation for LO worldwide. Although this feature has not been exploited in the present data set (narrow-band filters were inserted in some channels only to be used with other concurrent observations and gave a nonsignificant signal), it is our intention to do so in future observations. In addition to the obvious advantage of studying different astrophysical features of the source, e.g., measuring simultaneously the photospheric diameter and the height of a specific absorption layer in a late-type star, this multiwavelength approach also would provide us with a tool to disentangle source-specific light curve features from atmospheric noise. We recall that LO diffraction patterns are chromatic ($\propto \lambda^{-1/2}$) while scintillation is not (Roddier 1981). By

comparing light curves obtained with different filters for a source in which no wavelength variation is expected, we would then be able to significantly reduce the bias due to scintillation.

On the other hand, a potentially critical issue is the effect of pupil splitting on the light curves. It may affect the results of the analysis because of the possible effects induced on the fringes by the specific shape and reduction in size of the pupil. We investigated this issue comparing the results obtained combining the signals of all the channels (using the same filter on all of them) with those obtained analyzing them individually. No major effect caused by the pupil shape and no significant increment or decorrelation of the scintillation was found analyzing the data in one way or the other. It appears that, when analyzing the data separately, the decorrelation of the scintillation obtained averaging the data from the various channels is essentially compensated by the increase in the scintillation induced by the smaller pupil of each single channel.

Last but not least, the A/Iqueye instruments can be mounted at the 1.22 and 1.82 m telescopes simultaneously, and thus provide an opportunity for even more redundancy, wavelength filtering, and noise reduction. The linear distance between the two sites is ≈ 4 km: this has a negligible influence on the position angle at the Moon, but can make for a very significant difference in local limb slope, again providing a capability to disentangle source intrinsic from extrinsic effects.

4.1. Artificial Occulting Screens

The most striking feature of A/Iqueye, however, is the unparalleled ability to sample data with an extremely high time resolution. Here we shortly outline one possibility of exploiting this feature, suggesting to observe occultations by artificial screens in low orbit, such as the International Space Station (ISS). The advantages of such screens are multiple: they would make available sources outside the zodiacal belt, opening up all the sky visible from Asiago (north of decl. = -20°), which is at present impossible to study by LO; depending on the satellite orbit, they may allow us to repeat the observations several times; the events would occur in dark conditions, i.e., without the lunar background which is a dominant source of noise in LO; and finally, occultations by screens with multiple edges would permit true imaging, instead of 1D projections, using tomographic techniques.

The additional possibility of controlling the relative motion between the orbiting screen and the ground observer would also permit long integrations, which coupled with the aforementioned very low background would in turn enable an increase of many magnitudes over the present LO sensitivity level. Occultations by such space screens would thus permit us to break new ground in the study of extra-galactic sources and extra-solar planets with unprecedented angular resolution.

The manufacturing of artificial screens to be placed in orbit is currently starting, see, e.g., the development of solar sails for space propulsion such as for the near-Earth asteroid (NEA) Scout project (McNutt et al. 2014). However, the sizes needed for meaningful statistics of occultations and the need for steering them to occult specific targets make this a proposition still relatively far in the future.

Nevertheless, initial tests could be attempted already with structures available in space at present. Among them, the ISS is a perfect candidate, due to its relatively large angular size, and to its system of solar panels which are well suited to act as

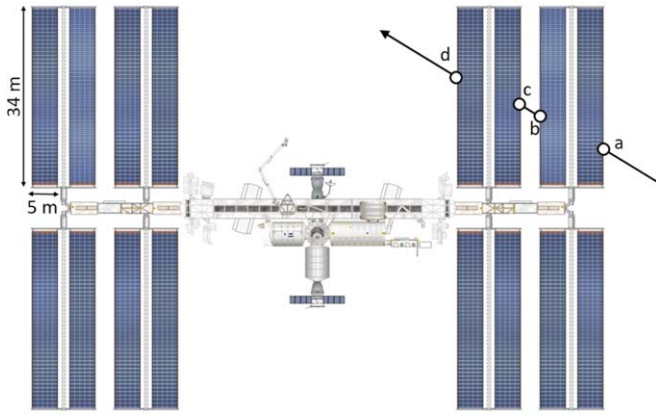


Figure 4. Occultations by the ISS. The letters mark the position where occultations on the solar panels occur. Adapted from historicspacecraft.com.

straight diffracting edges. See Figure 4 for layout and dimensions. The ISS orbit is at ≈ 400 km height. At this distance, Fresnel diffraction still applies (see Richichi & Glindemann 2012) and the main fringe has a width on the ground of ≈ 30 cm in the R band. From the ISS apparent speed of about 15.5 orbits day^{-1} it follows that the diffraction pattern would sweep a ground-based telescope at the rate of $\approx 2.5 \times 10^4$ fringes s^{-1} . Assuming to sample eight bins on the main fringe, this would require a read rate of about $5 \mu\text{s}$, which is entirely within the possibilities of A/Iqueye.

Of course, such rates would affect the sensitivity. Scaling from our detection of μ Psc ($R = 3.8$ mag) with $S/N = 25$ in a 3 nm FWHM filter with 2.5 ms, we estimate that, using Aqueye+ at the Copernicus telescope, with a broadband filter and a $5 \mu\text{s}$ sampling time, we should be able to record ISS occultations of stars with $R \lesssim 3$ mag, of which there are about 150 above the Asiago horizon. For stars of this brightness the count rate in a broadband filter should be reduced below the maximum rate sustainable by the acquisition electronics inserting an attenuator. This would in turn reduce the achievable S/N by a factor of ≈ 2 .

An estimate of the frequency of the occultations of a given star seen from Asiago (within $\pm 35''$, the average projected diagonal angular size of the ISS solar panels) shows that an event of this type will occur once every ~ 4.8 yr. This rate should be diminished by a factor of ~ 3 considering that half of the events occur during the day and that for a fraction of those occurring during the night the ISS would be sunlit. The potential rate of occultations of stars visible from Asiago with $R \lesssim 3$ mag is thus ~ 1 every 35 days.

Using Figure 4 as a reference, and neglecting for the moment additional effects due to the presence of the central station, it can be seen that depending on the geometry of approach there could be multiple occurrences of disappearance and reappearance events. In the figure, we show a case with a total of four events. The corresponding light curves would of course overlap in time, but their superposition would be linear and easily modeled. We show a simulation of this case in Figure 5.

Obviously there will be additional difficulties and limitations, e.g., the fact that the telescope aperture would be several times larger than the ground size of the main fringe or that observations should be done when the ISS is in eclipse to avoid contamination from reflected light, but in principle such events could be attempted already with A/Iqueye.

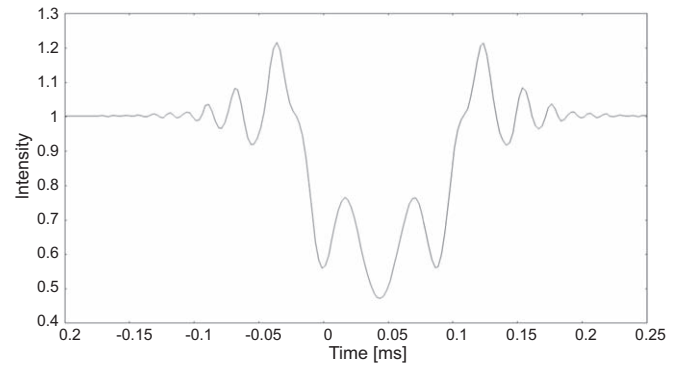


Figure 5. Simulation of an ISS occultation for the case considered in Figure 4.

Another interesting possibility for artificial screen occultations with fast photon counters is offered by geosynchronous satellites. At a higher altitude ($\approx 36,000$ km) and considerably smaller than the ISS, the probability of occultation by a single satellite is much lower but there are in fact hundreds of them visible from a single location. Although the diffraction patterns from such small screens might need specific numerical modeling, their slower angular motion (1 instead of 15 orbits day^{-1} , like the ISS) would enable the observer to use much longer sampling times, thus making the S/N /magnitude case favorable and possibly comparable to ISS occultations.

4.2. Occultations by Non-lunar Bodies

While not artificial, occultation events from the Saturnian ring plane recorded with the *Cassini* spacecraft represent a recent extension of the occultation technique to another non-lunar case (Stewart et al. 2013, 2015, 2016). Spatial information at extremely high angular resolution was recovered enabling a study of the stellar atmospheric extension across a spectral bandpass spanning the $1\text{--}5 \mu\text{m}$ spectral region.

The implementation of another very interesting non-LO technique has been recently reported by Benbow et al. (2019). They used fast photon-counting detectors on the 12 m VERITAS telescopes and an occulting asteroid to measure stellar diameters with an impressive resolution of ≤ 0.1 mas. The greater distance and, therefore, larger Fresnel pattern enabled larger telescope use with a corresponding increase in the source counting statistics and decrease in the scintillation.

This excellent new application of the occultation technique is however suitable mainly for very large telescopes because a large collecting area is needed to reach a significant S/N in a very short integration time and using narrow-band filters. The latter are required to avoid wavelength fringe smearing. In those rare cases in which a very bright star is occulted by an asteroid, also a 2 m class telescope equipped with a very fast photon-counting instrument like ours would of course be useful and certainly employed.

The scope of ISS and asteroidal occultations have some similarities, but also important scientific differences. Their statistics are in fact comparable, with the frequency of asteroidal occultations of any 10 mag star estimated at approximately 1 every 2 months and that of ISS occultations of any 3 mag star at one per month. Asteroidal occultations depend on the geometry of the asteroid, especially in the case of very small ones, while the geometry of the ISS is known. An additional advantage of the ISS is the number of scans. A single very large telescope will provide two light curves

(ingress and egress), while the ISS ingress/egress light curve pairs depend on the relative approach but could be as high as the number of panels (eight). Last but not least, asteroidal occultations aim mainly at faint stars with small diameters (typically <0.1 mas), i.e., either main-sequence stars (the diameters of which are already very well calibrated) or very far giant stars. ISS occultations aim mainly at bright stars, which are statistically much closer to the Sun, and of immediate scientific interest concerning, e.g., the investigation of stellar atmospheres and their immediate surroundings.

5. Conclusions

We reported the results of a novel program to observe LO that makes use of the two fast photometers Aqueye+ and Iqueye. During the period of 2016–2018 January, we observed a total of nine occultation events. For μ Psc we could measure for the first time the size of the chromosphere, while for the binary star SAO 92922 we obtained an additional measurement of the separation and position angle useful for reconstructing the properties of the orbit. We could also determine the angular diameter of α Tau, which we found in agreement with accepted literature values, albeit not with the accuracy required to investigate possible deviations from a symmetric disk model. However, fixing the lunar limb slope to the predicted value, the diameter in the H_α line turns out to be larger than the limb-darkened diameter and thus, as for μ Psc, we may have detected the chromosphere of the star.

The other stars were found to be unresolved, at the milliarcsecond level. We discuss the unique properties of Aqueye+ and Iqueye for these types of observations, namely the simultaneous measurement in up to four different filters thanks to pupil splitting, and the unprecedented time resolution well exceeding the microsecond level. This latter makes Aqueye+ and Iqueye suitable to observe not just occultations by the Moon, but also much faster events such as occultations by artificial screens in low orbits.

Finally, we mention that, in addition to LOs that constrain the properties of the far-away occulted target, occultations of stars by asteroids, Trans-Neptunian and/or Kuiper Belt objects can provide unique information on these nearby foreground objects (Camargo et al. 2018) and, despite being slower events, represent another promising area of potential future utilization of A/Iqueye.

We thank the referee for the useful comments. We would like to thank P. Favazza, L. Lessio, A. Siviero, A. Spolon, E. Verroi, and all the technical staff at the Asiago Cima Ekar and Pennar Observatories for their valuable operational support. We gratefully acknowledge also U. Munari for his independent suggestion of exploring the possibility of ISS occultations. L.Z. would like to thank Giovanni Caprara for sharing the exciting moments when the occultation of α Tau occurred, in a cold winter night, and Isacco M. Zampieri for the assistance in mounting and dismounting IFI+Iqueye. This work has made use of the SIMBAD database, operated at CDS, Strasbourg,

France. Based on observations collected at the Copernico telescope (Asiago, Italy) of the INAF—Osservatorio Astronomico di Padova and at the Galileo telescope (Asiago, Italy) of the University of Padova.

ORCID iDs

Luca Zampieri  <https://orcid.org/0000-0002-6516-1329>
 Andrea Richichi  <https://orcid.org/0000-0002-6554-9884>
 Mauro Barbieri  <https://orcid.org/0000-0001-8362-3462>

References

- Africano, J. L., Evans, D. S., Fekel, F. C., Smith, B. W., & Morgan, C. A. 1978, *AJ*, **83**, 1100
- Barbieri, C., Naletto, G., Occhipinti, T., et al. 2009, *JMOp*, **56**, 261
- Beavers, W. I., Cadmus, R. R., & Eitter, J. J. 1982, *AJ*, **87**, 818
- Bell, R. A., & Gustafsson, B. 1989, *MNRAS*, **236**, 653
- Benbow, W., Bird, R., Brill, A., et al. 2019, *NatAs*, **3**, 511
- Blackwell, D. E., Petford, A. D., Arribas, S., Haddock, D. J., & Selby, M. J. 1990, *A&A*, **232**, 396
- Camargo, J. I. B., Desmars, J., Braga-Ribas, F., et al. 2018, *P&SS*, **154**, 59
- Cohen, M., Walker, R. G., Carter, B., et al. 1999, *AJ*, **117**, 1864
- Davis, J., Tango, W. J., & Booth, A. J. 2000, *MNRAS*, **318**, 387
- Edwards, D. A., Evans, D. S., Fekel, F. C., & Smith, B. W. 1980, *AJ*, **85**, 478
- Gaia Collaboration, Brown, A. G. A., Vallenari, A., et al. 2018, *A&A*, **616**, A1
- Maksimov, A. F., Balega, Y. Y., Dyachenko, V. V., et al. 2009, *AstBu*, **64**, 296
- Mason, B. D. 1996, *AJ*, **112**, 2260
- Mason, B. D., Hartkopf, W. I., Holdenried, E. R., & Rafferty, T. J. 2001, *AJ*, **121**, 3224
- Mauas, P. J. D., Cacciari, C., & Pasquini, L. 2006, *A&A*, **454**, 609
- McNutt, L., Johnson, L., Clardy, D., et al. 2014, in *AIAA Space 2014 Conf.* (San Diego, CA: AIAA), 4435, <https://arc.aiaa.org/doi/abs/10.2514/6.2014-4435>
- McWilliam, A. 1990, *ApJS*, **74**, 1075
- Naletto, G., Barbieri, C., Occhipinti, T., et al. 2009, *A&A*, **508**, 531
- Naletto, G., Barbieri, C., Verroi, E., et al. 2013, *Proc. SPIE*, **8875**, 88750D
- Richichi, A. 1989, *A&A*, **226**, 366
- Richichi, A., di Giacomo, A., Lisi, F., & Calamai, G. 1992, *A&A*, **265**, 535
- Richichi, A., Dyachenko, V., Pandey, A. K., et al. 2017a, *MNRAS*, **464**, 231
- Richichi, A., Fors, O., Cusano, F., & Ivanov, V. D. 2014, *AJ*, **147**, 57
- Richichi, A., & Glindemann, A. 2012, *A&A*, **538**, A56
- Richichi, A., Percheron, I., & Khrstoforova, M. 2005, *A&A*, **431**, 773
- Richichi, A., & Roccatagliata, V. 2005, *A&A*, **433**, 305
- Richichi, A., Tasuya, O., Irawati, P., et al. 2016, *AJ*, **151**, 10
- Richichi, A., Tasuya, O., Irawati, P., & Yadav, R. K. 2017b, *AJ*, **154**, 215
- Ridgway, S. T., Jacoby, G. H., Joyce, R. R., Siegel, M. J., & Wells, D. C. 1982, *AJ*, **87**, 808
- Rodier, F. 1981, *PrOpt*, **19**, 281
- Schmidtke, P. C., & Africano, J. L. 1984, *AJ*, **89**, 1371
- Schmidtke, P. C., Africano, J. L., Jacoby, G. H., Joyce, R. R., & Ridgway, S. T. 1986, *AJ*, **91**, 961
- Stewart, P. N., Tuthill, P. G., Hedman, M. M., Nicholson, P. D., & Lloyd, J. P. 2013, *MNRAS*, **433**, 2286
- Stewart, P. N., Tuthill, P. G., Nicholson, P. D., & Hedman, M. M. 2016, *MNRAS*, **457**, 1410
- Stewart, P. N., Tuthill, P. G., Nicholson, P. D., Hedman, M. M., & Lloyd, J. P. 2015, *MNRAS*, **449**, 1760
- Verroi, E., Naletto, G., Barbieri, C., et al. 2013, *Proc. SPIE*, **8864**, 88641W
- Vieytes, M., Mauas, P., Cacciari, C., Origlia, L., & Pancino, E. 2011, *A&A*, **526**, A4
- Wenger, M., Ochsenbein, F., Egret, D., et al. 2000, *A&AS*, **143**, 9
- Zampieri, L., Naletto, G., Barbieri, C., et al. 2015, *Proc. SPIE*, **9504**, 95040C
- Zampieri, L., Naletto, G., Barbieri, C., et al. 2016, *Proc. SPIE*, **9907**, 99070N